universe

MDPI

Article

Variation in X_{CO} Factor in N55 Region

Qiang Li [1,2], Mingyue Li [2], Li Zhang [1,*] and Songpeng Pei [3]

1 College of Big Data and Information Engineering, Guizhou University, Guiyang 550025, China; nliqiang@foxmail.com
2 Qiannan Normal University for Nationalities, Duyun 558000, China
3 School of Physics and Electrical Engineering, Liupanshui Normal University, Liupanshui 553004, China; songpengpei@outlook.com
* Correspondence: lizhang.science@gmail.com

Abstract: The X_{CO} factor is defined as $X_{CO} = N(H_2)/W_{12CO}$. It is useful for estimating cloud mass. However, there is only limited research on how the X_{CO} factor varies within a single cloud. Employing $^{12}CO(J = 1\text{-}0)$ and $^{13}CO(J = 1\text{-}0)$ spectral data, we computed an X_{CO} factor of 3.6×10^{20} cm^{-2} (K km s^{-1})$^{-1}$ for luminous gas of the N55 region. Our analysis revealed a V-shaped correlation between the X_{CO} factor and H_2 column densities, while the relationship with excitation temperature exhibited obscurity. This suggests that the CO-to-H_2 conversion is not consistent on small scale (∼1 pc). Additionally, we found that star formation activity has little influence on the variability in the X_{CO} factor.

Keywords: interstellar medium; molecular clouds; Magellanic clouds

1. Introduction

The most abundant molecule in the universe is molecular hydrogen, H_2. Stars form out of clouds made of H_2, and the measurement of molecular hydrogen mass is fundamental to comprehending the star formation process [1,2]. While its spectrum of rotational transitions is not a good tracer of the mass in molecular clouds, due to requiring a high temperature to excite its rotational transitions, the emission of bulk H_2 in typical clouds is invisible [3]. Therefore, estimates of H_2 distribution need some indirect tracers. The lowest rotational transitions of the second most abundant molecule, $^{12}CO(1\text{-}0)$, have been considered the best tracers of molecular gas due to their strong line emission and easy observability. Due to these reasons, the relation between CO integrated intensity and H_2 column density is frequently used to measure the CO-to-H_2 conversion factor, X_{12CO} (hereafter, X_{CO}) [4]. This also makes the CO-to-H_2 conversion factor, X_{CO}, widely used for estimating cloud mass. The so-called X factor is formally defined as

$$X_{CO} = N(H_2)/W_{12CO}[\frac{\text{cm}^{-2}}{\text{K km s}^{-1}}], \tag{1}$$

where $N(H_2)$ is the H_2 column density, and W_{12CO} is the integrated $^{12}CO(J = 1\text{-}0)$ line intensity [5]. In mass units, Equation (1) can be rewritten as

$$\alpha_{CO} = M_{mol}/L_{12CO}[\frac{M_\odot}{\text{K km s}^{-1}\text{pc}^2}], \tag{2}$$

where M_{mol} is the total molecular mass. The relationship between X_{CO} and α_{CO} can be converted by a factor of 4.5×10^9 [6]. Various methods have been used to estimate the total gas mass, including those employing virial mass [7,8], dust emission or extinction [9–11], γ-ray emission [12–14], ^{13}CO [6,15], and [C *II*] [16–18].

Most studies of the X_{CO} factor consider an average value over a cloud and discuss the effects of cloud temperature, density, metallicity, and velocity dispersion on the X_{CO}

check for updates

Citation: Li, Q.; Li, M.; Zhang, L.; Pei, S. Variation in X_{CO} Factor in N55 Region. *Universe* **2024**, *10*, 200. https://doi.org/10.3390/universe10050200

Academic Editor: Keping Qiu

Received: 18 March 2024
Revised: 20 April 2024
Accepted: 26 April 2024
Published: 29 April 2024

factor [19–24]. Pineda et al. and Luo et al. [19,25] found that the X_{CO} factor in low-density regions without CO emission detections is six times higher than the average value in the Milky Way. Through analysis of positionally stacked spectra, Goldsmith et al. [26] suggested that low-intensity, yet large-area, emissions could significantly contribute to the CO emission in distant regions in our galaxy and in other galaxies. Papadopoulos et al. and Madden et al. [18,27] also demonstrate that the X_{CO} factor is exceptionally high in low-metallicity galaxies due to the effects of CO-dark gas. Ignoring metallicity effects, Maloney et al. [21] predicted $X_{CO} \propto T_K^{-1}$, but Shetty et al. [24] found a weaker $X - T_K$ dependence, $X_{CO} \propto T_K^{-0.5}$, where T_K represents kinetic temperature. Feldmann et al. and Bigiel et al. [20,28] predicted that the X_{CO} factor could vary by orders of magnitude in different environments.

However, only a few studies pay attention to variations in the X_{CO} factor within a single cloud (scale from ∼10 to ∼100 pc) [29–31]. Pineda et al. [30] showed that X_{CO} is heavily affected by the saturation of the emission above extinction A_V ∼4 mag. Sofue et al. and Kohno et al. [29,31] point out that the actual X_{CO} factor varies with the H_2 column density or with the CO line intensity in giant molecular clouds (GMCs). Therefore, more studies are needed to research the variation in the X_{CO} factor on a small scale.

Molecular clouds are surrounded by atomic envelopes and a transition region in which the hydrogen is primarily molecular, but the carbon is mostly atomic. These regions are known as photodissociation regions or photon-dominated regions (PDRs). More recently, they have been referred to as dark gas. Using analysis of positionally stacked spectra of the Taurus cloud, Goldsmith et al. [26] suggests a factor of two additional masses in this transition region. We also examine the effects of dark gas on the X_{CO} factor in other galaxies; hence, the N55 region was selected. N55 is located inside Large Magellanic Cloud 4 (LMC), the largest supergiant shell in the LMC. In this paper, we analyze the variation in the X_{CO} factor with H_2 column density and excitation temperature. We find that the CO-to-H_2 conversion is not universal on a small scale ∼1 pc. Additionally, we observe an uncertain correlation between the X_{CO} factor and excitation temperature. Furthermore, we find that the influence of star formation activity on the variation in the X_{CO} factor is minimal.

2. ALMA Archive Data

We use the Atacama Large Millimeter Array (ALMA) archive data of the N55 region in LMC, which is generated by the Additional Representative Image for Legacy (ARI-L) project [32]. The area of coverage was $4' \times 6'$ at the center position of ($05^h32^m15^s.49$, $-66^o26'14''.00$)(J2000). The synthesized beam for ^{12}CO(1-0) is approximately $3''.5 \times 2''.3$, and the position angle is 80.2°, which corresponds to 0.84 × 0.55 pc^2. The synthesized beam for ^{13}CO(1-0) is approximately $3''.8 \times 2''.7$, and the position angle is 69.8°, which corresponds to 0.91 × 0.65 pc^2. In order to compare these data sets pixel by pixel, we resample data with a common resolution. Finally, the pixel size is 0.49″ (∼0.1 pc). The rms σ per channel over 0.4 km s^{-1} is ∼57 mJy beam^{-1} and 18 mJy beam^{-1} for ^{12}CO(1-0) and ^{13}CO(1-0) (hereafter, ^{12}CO and ^{13}CO), respectively. We set zero values at the emission-free pixels ($<3\sigma$) to suppress the noise effect in our analysis. ^{12}CO emits beyond the area where ^{13}CO is detectable. Thus, comparing them pixel by pixel indicates that the following content is discussed for regions with detectable ^{13}CO ($>3\sigma$). Figure 1 shows ^{12}CO-integrated intensity map of these regions with detectable ^{13}CO emission ($>3\sigma$). Meanwhile, we examine the effects of noise on the X_{CO} factor and find that the error of only noise has little influence. Gruendl et al. and Seale et al. [33,34] identified 16 young stellar objects (YSOs) in the N55 region. The appearance of YSOs indicates ongoing star formation in these positions. The 13 YSOs are marked by red pluses in Figure 1.

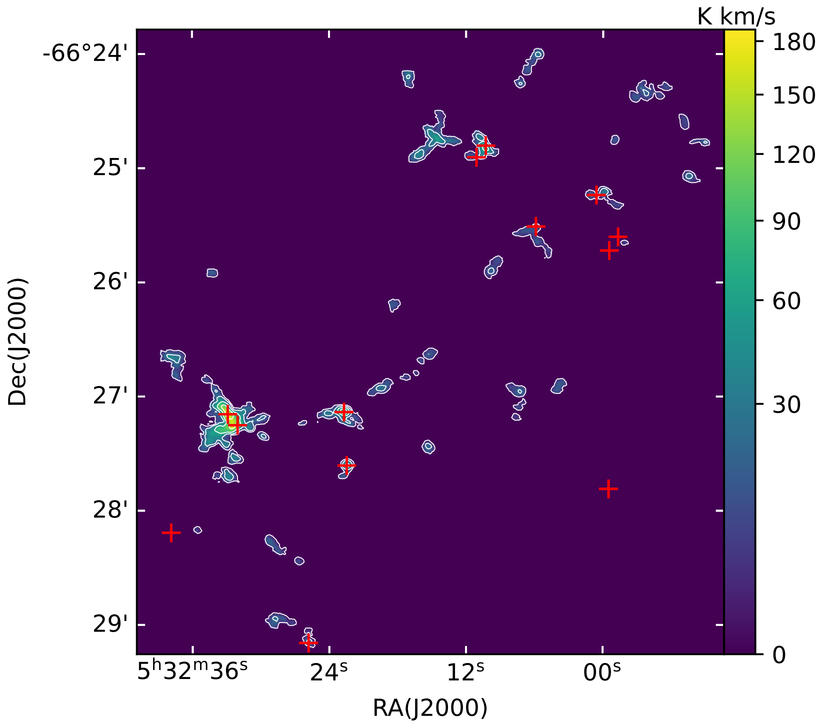

Figure 1. $^{13}CO(J = 1\text{-}0)$ emission in contours on $^{12}CO(J = 1\text{-}0)$-integrated intensity map of N55. The contour levels are 0.18, 1.6, 4.8, 9.6 K km s^{-1}. The red crosses are YSOs.

3. Data Analysis

According to the radiative transfer equation, the brightness temperature (T_B) is expressed in terms of the excitation temperature, T_{ex}, and optical depth, τ, as

$$T_B = T_0(\frac{1}{e^{T_0/T_{ex}} - 1} - \frac{1}{e^{T_0/T_{bg}} - 1})(1 - e^{-\tau})[\mathrm{K}], \tag{3}$$

where T_{bg} = 2.725 K and $T_0 = h\nu/k$ are the blackbody temperature of the cosmic background radiation and the Planck temperature, respectively.

We assumed that ^{12}CO is optically thick; then, $1 - e^{-\tau}$ tend to 1. We can rewrite Equation (3) as

$$T_B \approx T_0(\frac{1}{e^{T_0/T_{ex}} - 1} - \frac{1}{e^{T_0/T_{bg}} - 1})[\mathrm{K}]. \tag{4}$$

By equivalent transformation of Equation (4), the excitation temperature is written as

$$T_{ex} \approx 5.53194/ln(1 + \frac{5.53194}{T_{max}(^{12}CO) + 0.8632})[\mathrm{K}], \tag{5}$$

where 5.53194 K = $h\nu(^{12}CO)/k$, and $T_{max}(^{12}CO)$ is the main beam brightness temperature at the peak of ^{12}CO emission. The excitation temperature of our sample ranges from 5 to 42 K. Assuming optically thick causes higher values of our excitation temperature.

Assuming that the emission is in local thermodynamic equilibrium (LTE), the column density of ^{13}CO molecules is given by Sofue et al. [31]

$$N(^{13}CO) \approx 3 \times 10^{14} \frac{\tau}{1 - e^{-\tau}} \frac{1}{1 - e^{-5.28864/T_{ex}}} I_{^{13}CO}[\mathrm{cm}^{-2}], \tag{6}$$

where $I_{^{13}CO}$ is the ^{13}CO velocity-integrated intensity. Then, we calculate H_2 column density using

$$N(H_2) \approx Y(^{13}CO)N(^{13}CO)[\mathrm{cm}^{-2}], \tag{7}$$

where $Y(^{13}CO)$ is the abundance ratio of H_2 to ^{13}CO. We adopt abundance ratios of 50 for $[^{12}CO/^{13}CO]$ and 1.6×10^{-5} for $[^{12}CO/H_2]$ [35]. Hence, we obtain the abundance ratio of $Y(^{13}CO) = 3.125 \times 10^6$ and H_2 column density of

$$N(H_2) \approx 9.375 \times 10^{20} \frac{\tau}{1 - e^{-\tau}} \frac{1}{1 - e^{-5.28864/T_{ex}}} I_{^{13}CO} [\mathrm{cm}^{-2}]. \quad (8)$$

4. Results and Discussion

4.1. X_{CO} Factor

Fukui et al. [36] obtained an X_{CO} factor of 7×10^{20} cm^{-2}(K km s^{-1})$^{-1}$ for the LMC molecular clouds. Naslim et al. [2] gave a similar value of 6.5×10^{20} cm^{-2} (K km s^{-1})$^{-1}$ for N55 clumps in the LMC. However, Hughes et al. [37] reported a value of 4×10^{20} cm^{-2} (K km s^{-1})$^{-1}$. So, we try to calculate the factor by Equation (1). We may consider that ^{13}CO is optically thin and is a more natural tracer of the true column density. Using Equation (3) and assuming that the excitation temperature of ^{13}CO is equal to that of ^{12}CO, the optical depth can be calculated by

$$\tau(^{13}CO) \approx -ln(1 - \frac{T_{max}(^{13}CO)/5.28864}{(e^{5.28864/T_{ex}} - 1)^{-1} - 0.167667}), \quad (9)$$

where $T_{max}(^{13}CO)$ is the main beam brightness temperature at the peak of ^{13}CO emission. We calculate optical depth and excitation temperature in each cell (grid) of the channel maps at the line-center velocity. The calculated optical depth $\tau(^{13}CO)$ ranges from 0.03 to 0.58, with a mean value of 0.09, which suggests that ^{13}CO is nearly optically thin. The optically thin line is a more natural tracer of the true column density. So, we can calculate cloud mass using optically thin tracers.

Using Equation (9) and assuming that the excitation temperature of ^{13}CO is equal to that of ^{12}CO, we can obtain the optical depth of ^{13}CO. Then, we derive the H_2 column density by Equation (8). Finally, using Equation (1), we obtain a CO-to-H_2 conversion factor of 3.6×10^{20} cm^{-2} (K km s^{-1})$^{-1}$ for the entire region, which is similar to the value given by Hughes et al. [37]. It is interesting that there is a discrepancy between the two different ways (virial mass and LTE methods) for the X_{CO} factor. The result of the LTE method is smaller than the result of the virial mass method by a factor of 2. The discrepancy is similar to the result of Goldsmith et al. [26]. Using a column-density-dependent model for the CO fractional abundance, Goldsmith et al. [26] derive a mass more than twice as large as would be obtained using a canonical fixed fractional abundance of ^{13}CO. The gas mass from the virial mass method includes all media (CO luminous and dark gases), but the X_{CO} factor method only includes CO luminous gas. Our results suggest that the dark gas mass is close to the luminous gas mass.

The ^{12}CO emission traces the column density of molecular gas over a narrow dynamic range. It saturates at moderate column densities, as shown in a study by Kennicutt et al. [3]. We present plots of the calculated H_2 column densities using the X_{CO} and LTE methods in Figure 2. The H_2 column densities are calculated using $X_{CO} = 6.5 \times 10^{20}$ cm^{-2} (K km s^{-1})$^{-1}$ shown in Figure 2a, which shows almost no saturation in high-density regions. However, the H_2 column densities exhibit saturated values in high-density regions when using $X_{CO} = 3.6 \times 10^{20}$ cm^{-2} (K km s^{-1})$^{-1}$ shown in Figure 2b. Meanwhile, Sofue et al. and Pineda et al. [30,31] have reported saturated values of ^{12}CO in high-density regions of clouds. Therefore, $X_{CO} = 3.6 \times 10^{20}$ cm^{-2} (K km s^{-1})$^{-1}$ may be applicable for the N55 clumps.

We also examine the correlation between the mean column density $N(H_2)$ and the mean integrated ^{12}CO intensity W_{12CO} for each region in Figure 3. A least-squares linear fit is then performed, yielding a best-fit slope of $X_{CO} = (3.4 \pm 0.1) \times 10^{20}$ cm^{-2} (K km s^{-1})$^{-1}$, consistent with the value reported by Hughes et al. [37]. The slight discrepancy between the X_{CO} factor of the entire region, and each small region may be caused by different scales. We use Ramsey's reset test to find whether the relationship is non-linear. The F-test is statistically significant (p-value = 0.016), suggesting omitted variable bias. In other words, the non-linear relationship in Figure 3 exists. The typical scale of these single small regions is 1 pc. The non-linear relationship suggests that the fixed X_{CO} factor is unbefitting on a scale of $\sim$1 pc.

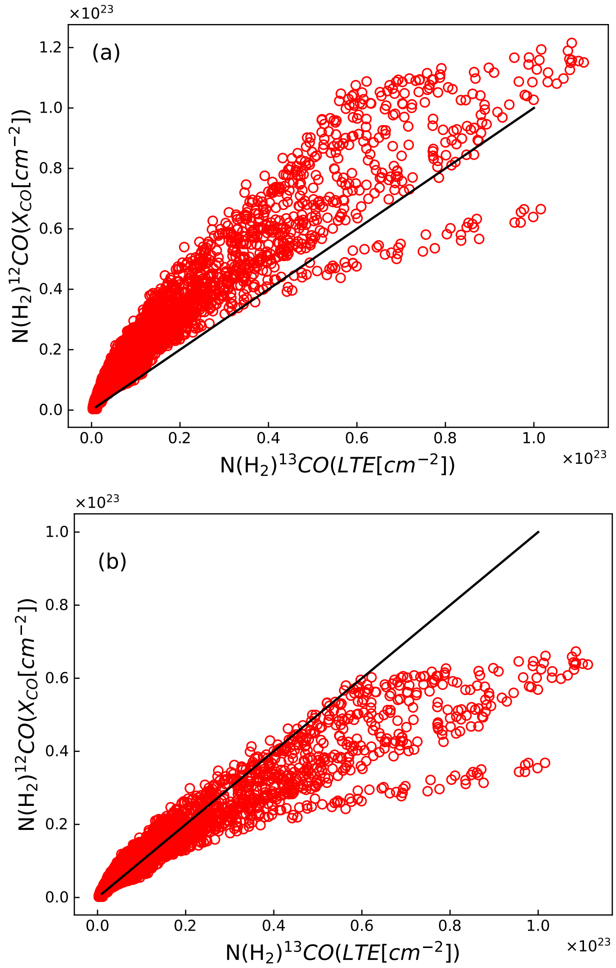

Figure 2. Plots of the calculated H_2 column densities using the X_{CO} and LTE methods for (**a**) $X_{CO} = 6.5 \times 10^{20}$ cm^{-2} (K km s^{-1})$^{-1}$ and (**b**) $X_{CO} = 3.6 \times 10^{20}$ cm^{-2} (K km s^{-1})$^{-1}$, respectively. The black solid lines indicate the linear relation of $N(H_2)(X_{CO}) = N(H_2)(LTE)$.

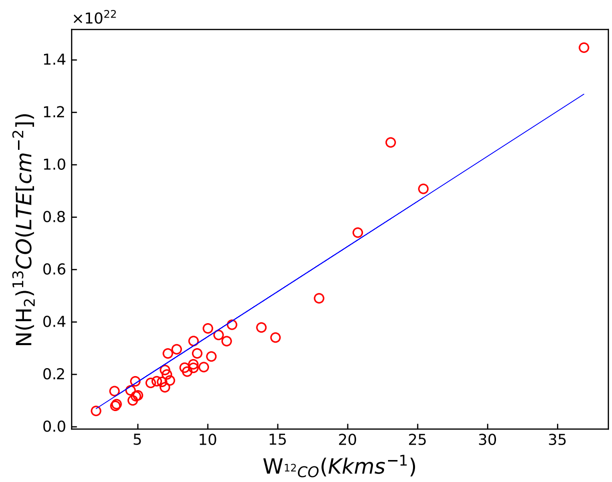

Figure 3. The mean column density $N(H_2)$ and mean integrated ^{12}CO intensity W_{12CO}. The blue line is best-fit X_{CO} factor for the N55 region, $X_{CO} = (3.4 \pm 0.1) \times 10^{20}$ cm^{-2} (K km s^{-1})$^{-1}$.

4.2. Variability in X_{CO} Factor

Regardless of the X_{CO} factor, Figure 2 shows the non-linear growth of the curve compared to the LTE method. We use Ramsey's reset test to find whether the relationship is non-linear. The F-test is statistically significant (p-value $\ll 0.001$), suggesting that there is omitted variable bias. In other words, the non-linear relationship in Figure 2 exists. This non-linear correlation implies that the X_{CO} factor is not constant at the pixel scale ($\sim$0.1 pc), and different X_{CO} factors are required. In Figure 4, plots of the distribution of the X_{CO} factor are shown. The X_{CO} factor varies within the range of $X_{CO}\sim(1.3–20.6) \times 10^{20}$ cm^{-2} (K km s^{-1})$^{-1}$.

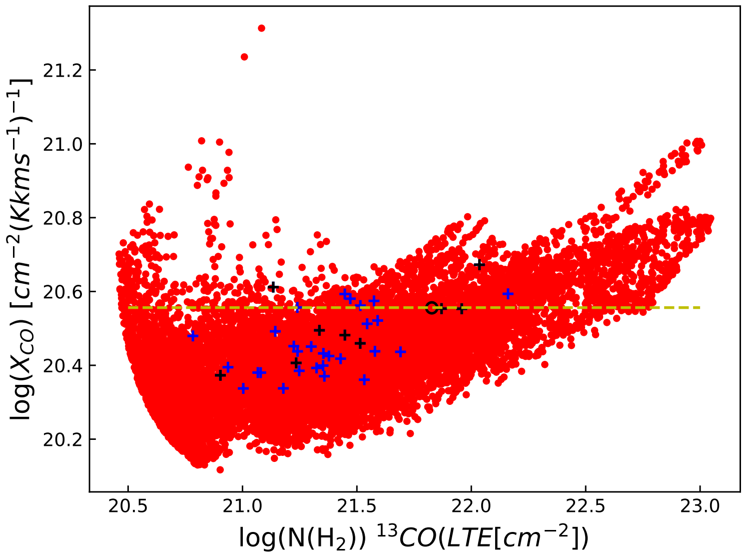

Figure 4. The plot of the distribution of the X_{CO} factor with column density $N(H_2)$. The black circle represents the entire region of N55. The plus symbols indicate the mean value in each region, with black and blue pluses representing clumps with and without YSOs, respectively. The yellow dashed line represents $X_{CO} = 3.6 \times 10^{20}$ cm^{-2} (K km s^{-1})$^{-1}$.

The plot of the X_{CO} factor and H_2 column densities shows a V-shaped behavior, with the turning point occurring at around 10^{21} cm^{-2}. The V-shaped behavior suggests a higher X_{CO} factor is needed at low H_2 density regions, as observed in [19,25]. At higher H_2 density regions, the X_{CO} factor increases with increasing column density. This can lead to underestimated or overestimated H_2 column densities if a fixed X_{CO} factor, usually derived from the mean value of the column density in individual molecular clouds or regions, is used. The V shape is due to the functional property of the "Q" function, as emphasized in reference [29,31]. Hence, the V shape is a general law of the transfer equation as a function of T_{ex} but does not express clouds.

We find that the distribution of X_{CO} factors for clumps with and without YSOs shows no significant differences in Figure 4, implying that star formation has little influence on determining the X_{CO} factor. Similar conclusions were drawn by Hughes et al. [37], where the difference in X_{CO} factors between young GMCs and other GMCs was only marginally significant. Additionally, Naslim et al. [2] found that molecular cores associated with YSOs generally exhibit larger linewidths and masses. The similarity in the distributions of X_{CO} factors between clumps with and without YSOs also suggests that the X_{CO} factor is insensitive to the velocity structure, which agrees with the results of Shetty et al. [24].

In Figure 5, we plot the X_{CO} factor as a function of excitation temperature for the entire region. We find that the X_{CO} factor decreases with increasing excitation temperature and exhibits a lower limit ranging from 1.3×10^{20} cm^{-2} (K km s^{-1})$^{-1}$ to 6×10^{20} cm^{-2} (K km s^{-1})$^{-1}$. However, this lower limit shows significant dispersion, with some pixels even showing a lack of convergence. To further investigate, we examine the correlation between the X_{CO} factor and excitation temperature for each clump. In Figure 6, we display the distribution of the X_{CO} factor for two clumps for contrast, while additional plots are provided in the Supplementary Materials. We find that these clumps show lower dispersion and different properties. one clump shows a V-shaped distribution of the X_{CO} factor, increasing with excitation temperature when $T_{ex} > 10$ K, while the other clump shows that the X_{CO} factor remains almost constant. Similarly, in the Supplementary Materials, some clumps show an increase in the X_{CO} factor with increasing excitation temperature, whereas others show a constant X_{CO} factor, suggesting an obscure correlation between the X_{CO} factor and excitation temperature. Additionally, the commonly observed lower transitions of CO are easily thermalized ($T_{ex} = T_K$). If we consider that the kinetic temperature is equal to the excitation temperature, this also suggests an obscure correlation between the X_{CO} factor and kinetic temperature. This is consistent with Kohno et al. [29] that there is no clear correlation between the X_{CO} factor and the $^{12}CO(J = 3\text{-}2/1\text{-}0)$ intensity ratio, which depends on the kinetic temperature.

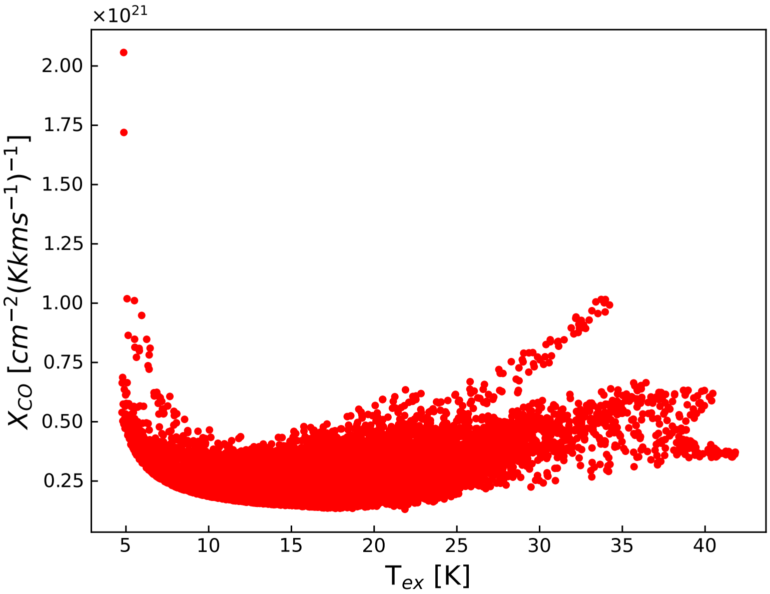

Figure 5. The plot of X_{CO} factors as functions of excitation temperature for the entire region.

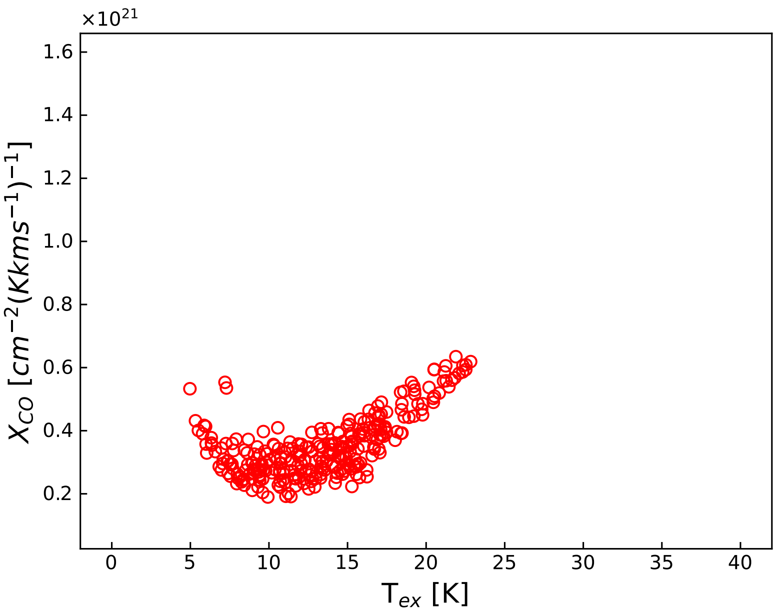

Figure 6. *Cont.*

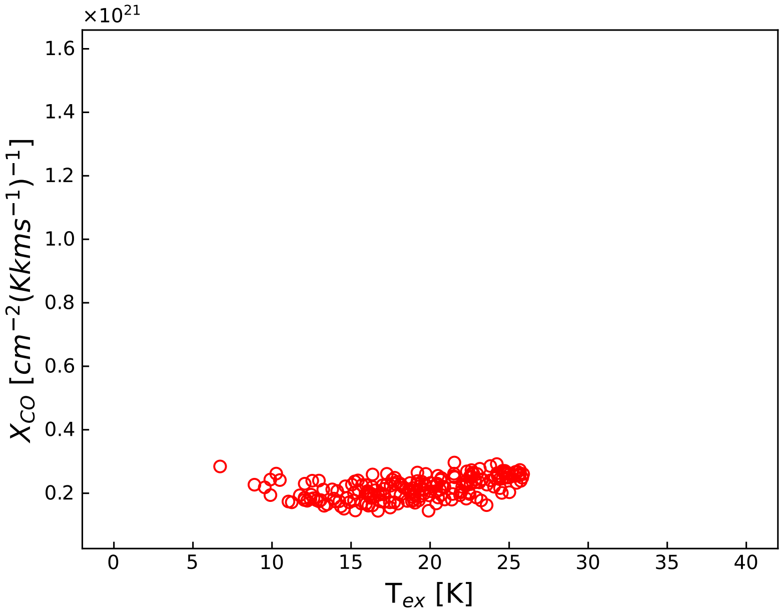

Figure 6. The plot of X_{CO} factors as functions of excitation temperature for each region. Only two clumps are showed, the rest parts are in Supplementary Materials.

5. Conclusions

Using ALMA spectral data, we computed an X_{CO} factor of 3.6×10^{20} cm^{-2} (K km s^{-1})$^{-1}$ for the N55 region in the LMC. Furthermore, we investigated the variation in the X_{CO} factor with H_2 column density and excitation temperature. The correlation between the X_{CO} factor and H_2 column densities reveals a V-shaped trend, while the relationship between the X_{CO} factor and excitation temperature exhibits obscurity. These findings suggest that the CO-to-H_2 conversion is not consistent on a small scale ($\sim$1 pc). Additionally, star formation activity appears to have minimal influence on the variation in the X_{CO} factor.

Supplementary Materials: The following supporting information can be downloaded at: https://www.mdpi.com/article/10.3390/universe10050200/s1, Figure S1 (1–37): The plot of X_{CO} factors as functions of excitation temperature for each region.

Author Contributions: Conceptualization, Q.L. and M.L.; formal analysis, Q.L. and M.L.; data curation, Q.L.; writing—original draft preparation, Q.L. and M.L.; writing—review and editing, Q.L., M.L., L.Z. and S.P. All authors have read and agreed to the published version of the manuscript.

Funding: The work was partially supported by the National Key *R&D* Program of China (No. 2022YFE0133700), the National Natural Science Foundation of China (No. 12273007, 11963003, 12242303), the National High-level Foreign Expert Recruitment Program (No. G2023038004), the Guizhou Provincial Excellent Young Science and Technology Talent Program (No. YQK[2023]006), the National SKA Program of China (No. 2020SKA0110300), the Guizhou Provincial Basic Research Program (Natural Science) (No. ZK[2022]143), the Cultivation project of Guizhou University (No. [2020]76), the Research Foundation of Qiannan Normal University for Nationalities (No. QNSY2019RC02), and the Science Research Project of University (Youth Project) of the department of education of Guizhou Province (QJJ[2022]348).

Data Availability Statement: The data are available from https://almascience.eso.org/aq/, accessed on 17 January 2020.

Acknowledgments: This paper makes use of the following ALMA data: ADS/JAO.ALMA#2013.1.00214.S. ALMA is a partnership of ESO (representing its member states), NSF (USA), and NINS (Japan), together with NRC (Canada), NSTC and ASIAA (Taiwan), and KASI (Republic of Korea), in cooperation with the Republic of Chile. The Joint ALMA Observatory is operated by ESO, AUI/NRAO, and NAOJ.

Conflicts of Interest: The authors declare no conflicts of interest.

Abbreviations

The following abbreviations are used in this manuscript:

PDR	Photodissociation region
GMC	Giant molecular cloud
ALMA	Atacama Large Millimeter Array
LMC	Large Magellanic Cloud
LTE	Local thermodynamic equilibrium
ART−L	Additional Representative Image for Legacy
YSO	Young stellar object

References

1. Fukui, Y.; Kawamura, A. Molecular Clouds in Nearby Galaxies. *Annu. Rev. Astron. Astrophys.* **2010**, *48*, 547–580. [CrossRef]
2. Naslim, N.; Tokuda, K.; Onishi, T.; Kemper, F.; Wong, T.; Morata, O.; Takada, S.; Harada, R.; Kawamura, A.; Saigo, K.; et al. ALMA Reveals Molecular Cloud N55 in the Large Magellanic Cloud as a Site of Massive Star Formation. *Astrophys. J.* **2018**, *853*, 175.
3. Kennicutt, R.C.; Evans, N.J. Star Formation in the Milky Way and Nearby Galaxies. *Annu. Rev. Astron. Astrophys.* **2012**, *50*, 531. [CrossRef]
4. Solomon, P.M.; Rivolo, A.R.; Barrett, J.; Yahil, A. Mass, Luminosity, and Line Width Relations of Galactic Molecular Clouds. *Astrophys. J.* **1987**, *319*, 730. [CrossRef]
5. Bolatto, A.D.; Wolfire, M.; Leroy, A.K. The CO-to-H_2 Conversion Factor. *Annu. Rev. Astron. Astrophys.* **2013**, *51*, 207–268. [CrossRef]
6. Teng, Y.H.; Sandstrom, K.M.; Sun, J.; Leroy, A.K.; Johnson, L.C.; Bolatto, A.D.; Kruijssen, J.M.D.; Schruba, A.; Usero, A.; Barnes, A.T.; et al. Molecular Gas Properties and CO-to-H_2 Conversion Factors in the Central Kiloparsec of NGC 3351. *Astron. Astrophys.* **2022**, *925*, 72. [CrossRef]
7. Bolatto, A.D.; Leroy, A.K.; Rosolowsky, E.; Walter, F.; Blitz, L. The Resolved Properties of Extragalactic Giant Molecular Clouds. *Astrophys. J.* **2008**, *686*, 948–965. [CrossRef]
8. Donovan, M.J.; Koda, J.; Momose, R.; Mooney, T.; Egusa, F.; Carty, M.; Kennicutt, R.; Kuno, N.; Rebolledo, D.; Sawada, T.; et al. Resolved Giant Molecular Clouds in Nearby Spiral Galaxies: Insights from the CANON CO (1-0) Survey. *Astrophys. J.* **2013**, *772*, 107. [CrossRef]
9. Imara, N. Rethinking a Mysterious Molecular Cloud. *Astrophys. J.* **2015**, *803*, 38. [CrossRef]
10. Leroy, A.K.; Bolatto, A.; Gordon, K.; Sandstrom, K.; Gratier, P.; Rosolowsky, E.; Engelbracht, C.W.; Mizuno, N.; Corbelli, E.; Fukui, Y.; et al. The CO-to-H_2 Conversion Factor from Infrared Dust Emission across the Local Group. *Astrophys. J.* **2011**, *737*, 12. [CrossRef]
11. Planck Collaboration; Ade, P.A.R.; Aghanim, N.; Arnaud, M.; Ashdown, M.; Aumont, J.; Baccigalupi, C.; Balbi, A.; Banday, A.J.; Barreiro, R.B.; et al. Planck early results. XIX. All-sky temperature and dust optical depth from Planck and IRAS. Constraints on the "dark gas" in our Galaxy. *Astron. Astrophys.* **2011**, *536*, 19.
12. Abdo, A.A.; Ackermann, M.; Ajello, M.; Baldini, L.; Ballet, J.; Barbiellini, G.; Bastieri, D.; Baughman, B.M.; Bechtol, K.; Bellazzini, R.; et al. Fermi Observations of Cassiopeia and Cepheus: Diffuse Gamma-ray Emission in the Outer Galaxy. *Astrophys. J.* **2010**, *710*, 133–149. [CrossRef]
13. Ackermann, M.; Ajello, M.; Allafort, A.; Baldini, L.; Ballet, J.; Barbiellini, G.; Bastieri, D.; Belfiore, A.; Bellazzini, R.; Berenji, B.; et al. The cosmic-ray and gas content of the Cygnus region as measured in γ-rays by the Fermi Large Area Telescope. *Astron. Astrophys.* **2012**, *538*, 71. [CrossRef]
14. Remy, Q.; Grenier, I.A.; Marshall, D.J. Cosmic rays, gas and dust in nearby anticentre clouds. I. CO-to-H_2 conversion factors and dust opacities. *Astron. Astrophys.* **2017**, *601*, 78. [CrossRef]
15. Cormier, D.; Bigiel, F.; Jimenez-Donaire, M.J.; Leroy, A.K.; Gallagher, M.; Usero, A.; Sandstrom, K.; Bolatto, A.; Hughes, A.; Kramer, C.; et al. Full-disc 13CO(1-0) mapping across nearby galaxies of the EMPIRE survey and the CO-to-H_2 conversion factor. *Mon. Not. R. Astron. Soc.* **2018**, *475*, 3909–3933. [CrossRef]
16. Accurso, G.; Saintonge, A.; Catinella, B.; Cortese, L.; Dave, R.; Dunsheath, S.H.; Genzel, R.; Gracia-Carpio, J.; Heckman, T.M.; Jimmy; et al. Deriving a multivariate α_{CO} conversion function using the [C *II*]/CO (1-0) ratio and its application to molecular gas scaling relations. *Mon. Not. R. Astron. Soc.* **2017**, *470*, 4750–4766.
17. Bigiel, F.; de Looze, I.; Krabbe, A.; Cormier, D.; Barnes, A.T.; Fischer, C.; Bolatto, A.D.; Bryant, A.; Colditz, S.; Geis, N.; et al. SOFIA/FIFI-LS Full-disk [C *II*] Mapping and CO−dark Molecular Gas across the Nearby Spiral Galaxy NGC 6946. *Astrophys. J.* **2020**, *903*, 30. [CrossRef]
18. Madden, S.C.; Cormier, D.; Hony, S.; Lebouteiller, V.; Abel, N.; Galametz, M.; De Looze, I.; Chevance, M.; Polles, F.L.; Lee, M.-Y.; et al. Tracing the total molecular gas in galaxies: [C *II*] and the CO-dark gas. *Astron. Astrophys.* **2020**, *643*, 141. [CrossRef]
19. Luo, G.; Li, D.; Tang, N.; Dawson, J.R.; Dickey, J.M.; Bronfman, L.; Qin, S.-L.; Gibson, S.J.; Plambeck, R.; Finger, R.; et al. Revealing the CO X-factor in Dark Molecular Gas through Sensitive ALMA Absorption Observations. *Astron. J.* **2020**, *889*, 4. [CrossRef]
20. Feldmann, R.; Gnedin, N.Y.; Kravtsov, A.V. The X-factor in Galaxies. I. Dependence on Environment and Scale. *Astrophys. J.* **2012**, *747*, 124. [CrossRef]

21. Maloney, P.; Black, J.H. I CO/N(H_2) Conversions and Molecular Gas Abundances in Spiral and Irregular Galaxies. *Astrophys. J.* **1988**, *325*, 389. [CrossRef]
22. Narayanan, D.; Krumholz, M.R.; Ostriker, E.C.; Hernquist, L. A general model for the CO-H_2 conversion factor in galaxies with applications to the star formation law. *Mon. Not. R. Astron. Soc.* **2012**, *421*, 3127–3146. [CrossRef]
23. O'Neill, T.J.; Indebetouw, R.; Sandstrom, K.; Bolatto, A.D.; Jameson, K.E.; Carlson, L.R.; Finn, M.K.; Meixner, M.; Sabbi, E.; Sewilo, M. Sequential Star Formation in the Young SMC Region NGC 602: Insights from ALMA. *Astrophys. J.* **2022**, *938*, 82. [CrossRef]
24. Shetty, R.; Glover, S.C.; Dullemond, C.P.; Ostriker, E.C.; Harris, A.I.; Klessen, R.S. Modelling CO emission-II. The physical characteristics that determine the X factor in Galactic molecular clouds. *Mon. Not. R. Astron. Soc.* **2011**, *415*, 3253–3274. [CrossRef]
25. Pineda, J.L.; Goldsmith, P.F.; Chapman, N.; Snell, R.L.; Li, D.; Cambresy, L.; Brunt, C. The Relation Between Gas and Dust in the Taurus Molecular Cloud. *Astrophys. J.* **2010**, *721*, 686–708. [CrossRef]
26. Goldsmith, P.F.; Heyer, M.; Narayanan, G.; Snell, R.; Li, D.; Brunt, C. Large-Scale Structure of the Molecular Gas in Taurus Revealed by High Linear Dynamic Range Spectral Line Mapping. *Astrophys. J.* **2008**, *680*, 428–445. [CrossRef]
27. Papadopoulos, P.P.; Padelis, P.; Bisbas, T.G.; Zhang, Z.-Y. New places and phases of CO-poor/C *I*-rich molecular gas in the Universe. *Mon. Not. R. Astron. Soc.* **2018**, *478*, 1716–1725. [CrossRef]
28. Gong, M.; Ostriker, E.C.; Kim, C.-G.; Kim, J.-G. The Environmental Dependence of the X_{CO} Conversion Factor. *Astrophys. J.* **2020**, *903*, 142. [CrossRef]
29. Kohno, M.; Sofue, Y. The CO-to-H_2 conversion factor of Galactic giant molecular clouds using CO isotopologues: High-resolution X_{CO} maps. *Mon. Not. R. Astron. Soc.* **2024**, *527*, 9290–9302. [CrossRef]
30. Pineda, J.E.; Caselli, P.; Goodman, A.A. CO Isotopologues in the Perseus Molecular Cloud Complex: The X-factor and Regional Variations. *Astrophys. J.* **2008**, *679*, 481–496. [CrossRef]
31. Sofue, Y.; Kohno, M. CO-to-H_2 conversion and spectral column density in molecular clouds: The variability of the X_{CO} factor. *Mon. Not. R. Astron. Soc.* **2020**, *497*, 1851–1861. [CrossRef]
32. Massardi, M.; Stoehr, F.; Bendo, G.J.; Bonato, M.; Brand, J.; Galluzzi, V.; Guglielmetti, F.; Liuzzo, E.; Marchili, N.; Richards, A.M.S.; et al. The Additional Representative Images for Legacy (ARI-L) Project for the ALMA Science Archive. *Publ. Astron. Soc. Pac.* **2021**, *133*, 1026. [CrossRef]
33. Gruendl, R.A.; Chu, Y.-H. High- and Intermediate-Mass Young Stellar Objects in the Large Magellanic Cloud. *Astrophys. J. Suppl.* **2009**, *184*, 172–197. [CrossRef]
34. Seale, J.P.; Meixner, M.; Sewilo, M.; Babler, B.; Engelbracht, C.W.; Gordon, K.; Hony, S.; Misselt, K.; Montiel, E.; Okumura, K.; et al. Herschel Key Program Heritage: A Far-Infrared Source Catalog for the Magellanic Clouds. *Astron. J.* **2014**, *148*, 124. [CrossRef]
35. Mizuno, Y.; Kawamura, A.; Onishi, T.; Minamidani, T.; Muller, E.; Yamamoto, H.; Hayakawa, T.; Mizuno, N.; Mizuno, A.; Stutzki, J.; et al. Warm and Dense Molecular Gas in the N 159 Region: $^{12}CO J = $ 4-3 and $^{13}CO J = $ 3-2 Observations with NANTEN2 and ASTE. *Astron. Astrophys.* **2010**, *62*, 51–67. [CrossRef]
36. Fukui, Y.; Kawamura, A.; Minamidani, T.; Mizuno, Y.; Kanai, Y.; Mizuno, N.; Onishi, T.; Yonekura, Y.; Mizuno, A.; Ogawa, H.; et al. Mass, The Second Survey of the Molecular Clouds in the Large Magellanic Cloud by NANTEN. I. Catalog of Molecular Clouds. *Astrophys. J. Suppl. Ser.* **2008**, *178*, 56–70. [CrossRef]
37. Hughes, A.; Wong, T.; Ott, J.; Muller, E.; Pineda, J.L.; Mizuno, Y.; Bernard, J.-P.; Paradis, D.; Maddison, S.; Reach, W.T.; et al. Physical properties of giant molecular clouds in the Large Magellanic Cloud. *Mon. Not. R. Astron. Soc.* **2010**, *406*, 2065–2086. [CrossRef]